

A generalized multi-particle drift-diffusion simulator for optoelectronic devices

Daniele Rossi[†], Matthias Auf der Maur^{†,*}, Aldo Di Carlo[†]

[†]Dept. of Electronic Engineering, Università degli Studi di Roma “Tor Vergata”, Via del Politecnico 1, 00133 Rome, Italy

*Email: auf.der.maur@ing.uniroma2.it

Abstract—We present a generalized multi-particle drift-diffusion model capable to overcome the limitations imposed by the classic drift-diffusion model. It was designed as flexible and reusable tool that takes into account explicitly multiple carrier populations, whether charged and neutral, allowing to consider also e.g. exciton transport or ionic motion, crucial for a relevant number of device structures.

Index Terms—Band-to-band transition, drift-diffusion, exciton transport, ion migration, organic light emitting diodes (OLEDs), organic optoelectronic, semiconductor device modeling.

I. INTRODUCTION

The simulation of electronic devices is nowadays a task that requires to go far beyond the simple picture of semiconductors with electrons and holes transport in corresponding bands. In the last two decades several applications have been intensively studied and developed. Indeed, devices as organic light emitting diodes (OLEDs), organic photovoltaics (OPVs) and organic field effect transistors (OFETs), exhibit complex electronic properties due to the presence of amorphous or regular assembly of polymer/small molecules in such materials. Besides electrons and holes, in devices for OPVs, such as dye-sensitized solar cells (DSSCs) and perovskite solar cells (PSCs), the ions transport plays a role in the device operation.

The traditional approach for semiconductor transport modeling in electronic devices is based on semi-classical transport equations known as drift-diffusion model (DD), or the van Roosbroeck equations [1]. In the DD model the set of equations is formulated for an electron and a hole population, assumed each in local thermal equilibrium with the host material.

Due to the complexity of mechanisms involved in new technology devices, over the years, several extensions of the DD model have been developed, but they are particularly designed for specific situations, such as for transport modeling in quantum dots (QDs) [2], or in multi quantum wells (MQWs) LEDs simulation [3].

The purpose of this work is to formulate and implement a generalization of the semi-classical drift-diffusion model extendible for multi-particle systems, flexible enough to allow the investigation of a wide range of devices for which this modeling is applicable.

II. THE MODEL

We propose a multi-particle drift-diffusion model (mp-DD) [4] that allows to overcome all limitations imposed by

having only two-carrier transport model, as in traditional drift-diffusion. This is done by splitting the total particle population of the system into sub-populations, that are weakly coupled with each other compared to the corresponding relaxation time. The modeling approach is based on two ingredients:

- the model is extended to more than two carriers population, each individually assumed in a local thermal equilibrium and characterized by a local quasi-Fermi level;
- transitions between populations are formulated with strictly thermodynamic consistency, appearing as generation-recombination terms in the coupled system of equations.

The mp-DD allows to define any number of carriers, each one with its own properties, as spin, charge and density of states (DOS). Sticking to the stationary case, the system of equations reads as

$$\nabla \cdot (\varepsilon_0 \varepsilon_r \nabla \varphi - \mathbf{P}_0) = -q \sum_i z_i n_i - qC \quad (1a)$$

$$\nabla \cdot (\mu_i n_i \nabla \phi_i) = \text{sgn}(z_i) R_i, \quad \forall i. \quad (1b)$$

The Poisson equation in Eq. (1a) is used to calculate the electrostatic potential φ by considering the overall charged carrier densities and fixed charges, respectively indicated by n_i and C . z_i and q represent the i -th carriers charge number and the elementary charge, while \mathbf{P}_0 indicates the fixed polarization that models e.g. piezoelectric and spontaneous polarization. The set of continuity equations in Eq. (1b) describes the transport of all carriers included in the system, both charged and neutral. On the left side of Eq. (1b), the carrier flux is written in terms of gradient of the quasi-Fermi potential ϕ_i , μ_i is the carrier mobility, while the term $\text{sgn}(z_i)$ adjusts the sign according to the definition of the quasi-Fermi potential as $-q\phi_i = E_{F,i}$. The term R_i is the total recombination-generation rate of the i -th carrier and generally depends on different carrier densities (n_i), therefore couples different carrier populations.

The implementation is done using quasi-Fermi potentials as primary variables so that we do not need to explicitly use the generalized Einstein relation, or specially treat spatial dependent material properties.

$$n_i = \int_{-\infty}^{\infty} D_i(E) \frac{1}{\exp\left(\frac{E + \text{sgn}(z_i)q\phi_i - z_i q\varphi}{k_B T}\right) \pm 1} dE. \quad (2)$$

Here, $D_i(E)$ represents the DOS of the i -th carrier, while \pm denotes the possibility to use of both the Fermi-Dirac and Bose-Einstein statistics. The latter is required in order to describe quasi-particles like excitons, thus z_i can be also 0. In analogy to chemistry, all recombination/generation rates are written as reactions between different species in the system.

$$\sum_j \alpha_j n_j \rightleftharpoons 0 \rightarrow \sum_j \alpha_j \phi_j = 0 \quad (3a)$$

$$r_i = \alpha_i \left[1 - e^{-\frac{q}{k_B T} \sum_j \alpha_j \phi_j} \right] \sum_{\{\theta_j\}} \gamma(\{\theta_j\}) \times \prod_j \left[\frac{1}{2} (1 - \text{sgn}(\alpha_j)) \pm f_j(\theta_j) \right]^{|\alpha_j|}. \quad (3b)$$

Equation (3a) shows the reaction and the corresponding thermodynamic equilibrium condition in the isothermal case. Here, α_j is an integer that represents the stoichiometric coefficient of the j -th particle, which determines the number of particles involved in the reaction for population j . Furthermore, its sign determines whether the particle is destroyed or generated in the reaction.

Equation (3b) originates from the inter-band scattering terms appearing in the Boltzmann transport equation, using however equilibrium distribution functions. It gives the general expression for the net recombination rate of a specific recombination process in which the i -th carrier is involved, such that $R_i = \sum r_i$. $f_j(\theta_j)$ is the equilibrium distribution of carrier j , depending on a set of degree of freedoms (θ_j), like e.g. spin or crystal momentum. From Eq. (3b) any recombination model can be derived, e.g. from the simple radiative decay of excitons up to three-carriers mechanisms such as Auger recombination [4]. The model is implemented in the simulation software TiberCAD [5] using the Galerkin finite element method (FEM), and calculates solutions of the non-linear equations with Newton method.

In the following, we present two different contexts where the multi-particle drift-diffusion model can be exploited.

III. SIMULATION OF PHOSPHORESCENT OLED

The need of very wide bandgap and the short lifetime of the blue emitters limit the performance of RGB OLED displays. For this reason, the fabrication of highly efficient deep-blue OLEDs is quite challenging. Since the first attempt of OLED fabrication [6], over the years further attempts have been done. The second-generation OLEDs, based on phosphorescent emitters, represent one of the most common design strategies employed for blue-emission. This technology exploits the inclusion of organometallic complexes to harvest both singlet (S) and triplet (T) excited states by enhancing the spin-orbit coupling (SOC). It allows ideally achieving nearly

100% IQE and EQE $\simeq 19\%$, as demonstrated by Adachi et al. [7] in 2001.

Here we model both the electrical and optical operation of a typical phosphorescent OLED, as depicted in Fig. 1.

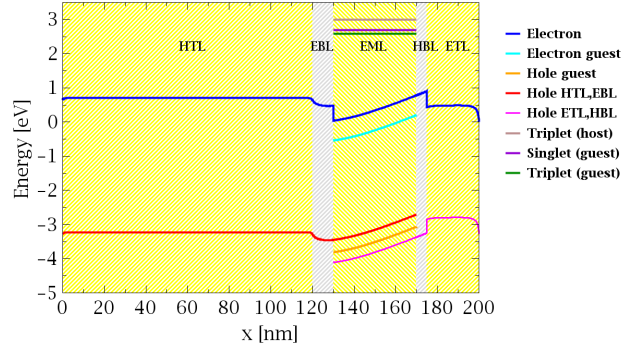


Fig. 1. Energy levels of carrier sub-populations included in the PHOLED system: respectively 12 electrons/holes and 3 excitons singlet/triplets

The emitter (EML) consists of a host-guest matrix system made by the mixture of EBL, HBL and guest materials (with a molar ratio of 70:20:10). The energy levels alignment is designed as it to foster the inter-system crossing (ISC) process contributing to the phosphorescent emission through triplets radiative decay. The structure is completed by 2 blocking/transport layers for the electrons and holes injection. In each material, we include carrier populations by explicitly defining their own properties as charge, spin and DOS. Given the organic nature of materials, we include the molecular disorder for both charged and neutral carriers by using Gaussian DOS profiles centered in the HOMO and LUMO levels. The charge transfer rate (R_{bb^*}) between host and guest populations is accounted by using the following band-to-band recombination model

$$R_{bb^*} = C_{bb^*} n_b \left(1 - \frac{n_{b^*}}{N_{b^*}} \right) \left[1 - \exp\left(\frac{E_{f,b^*} - E_{f,b}}{k_B T} \right) \right]. \quad (4)$$

Here, the constant rate C_{bb^*} regulates the rate of transitions depending on the carrier concentrations (n_b, n_{b^*}) and corresponding quasi-Fermi energy levels ($E_{f,b}, E_{f,b^*}$), while N_{b^*} represents the overall number of available states. For this system we set $C_{EBL, guest} = 10^{-13} \text{ cm}^3 \cdot \text{s}^{-1}$, $C_{HBL, guest} = 10^{-10} \text{ cm}^3 \cdot \text{s}^{-1}$ and $C_{EBL, guest} = 10^{-14} \text{ cm}^3 \cdot \text{s}^{-1}$.

Concerning excitons, we consider $T_1(\text{h}) = 2.84 \text{ eV}$, $S_1(\text{g}) = 2.56 \text{ eV}$ and $T_1(\text{g}) = 2.49 \text{ eV}$ and we model the related radiative (τ) and non-radiative (nr) decay processes. Figure 2(a) shows schematically all main kinetic mechanisms included in the simulations involving excitons.

The emission is due to the triplets radiative decay and it is aided by ISC that allows increasing the triplet density (n_T) available. We model this process with

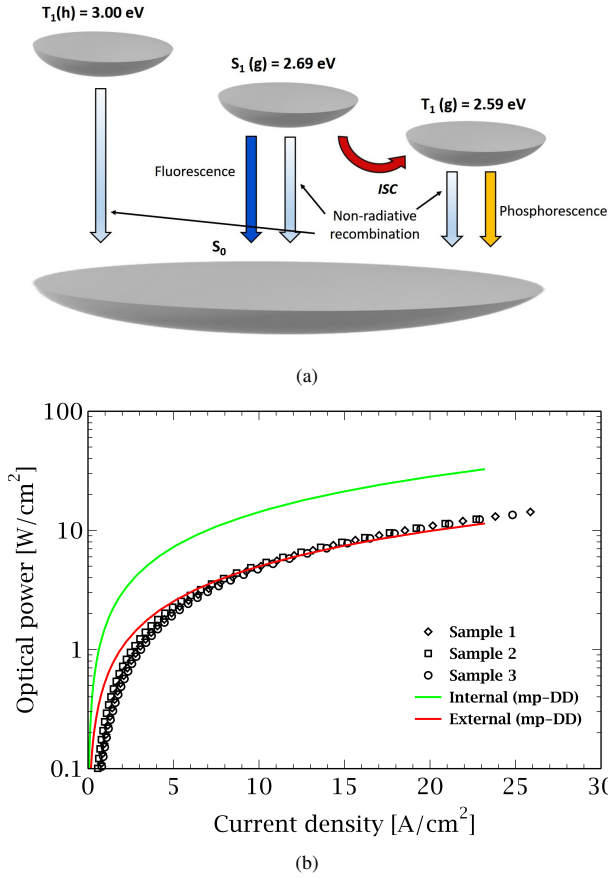


Fig. 2. a) Scheme of exciton states and decay rates accounted within the host-guest system. The exciton decay processes are modeled by setting: $\tau_{nr,T_1}(h)=10^{-6}$ s, $\tau_{rr,S_1}(g)=10^{-9}$ s, $\tau_{nr,S_1}(g)=10^{-9}$ s, $\tau_{rr,T_1}(g)=10^{-6}$ s and $\tau_{nr,T_1}(g)=10^{-4}$ s; b) internal and external optical power comparison between experimental results and mp-DD calculations.

$$R_{ISC} = C_{ISC} n_S \left(1 + \frac{n_T}{N_T} \right) \left[1 - \exp \left(\frac{E_{f,T} - E_{f,S}}{k_B T} \right) \right], \quad (5)$$

where, n_S indicates the singlet density, $E_{f,T}, E_{f,S}$ the quasi-Fermi levels of both exciton species and C_{ISC} represents the constant rate, for which we set a value of 10^{-11} $\text{cm}^3 \cdot \text{s}^{-1}$. The exciton generation is then included using constant rates $C_G(h)=C_G(g)=10^{-22}$ $\text{cm}^3 \cdot \text{s}^{-1}$, and respecting the typical 1:3 ratio between singlets and triplets according to spin statistics.

We examined the device operation and we calculated the optical power generated internally at different current density bias. From comparison shown in Fig. 2(b), the internal optical power (red) is quite consistent with the curve trend of the external optical powers experimentally measured (black symbols). Furthermore, we calculated a light extraction efficiency (LEE) of around 35%, that allows to obtain a reasonable match with experimental results on the external optical power. This calculation is roughly done by assuming that LEE is constant

for both $\lambda_{S_1}=461$ nm and $\lambda_{T_1}=479$ nm.

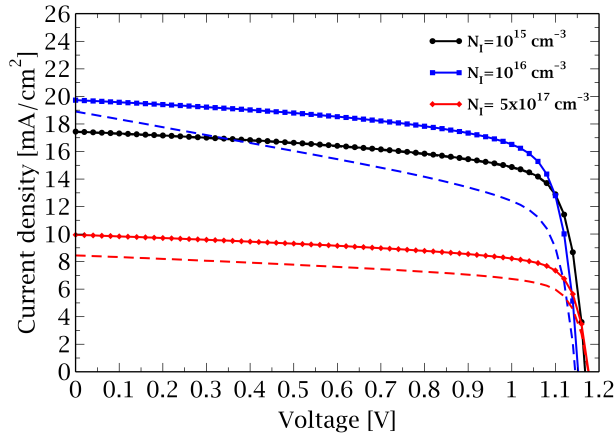
IV. ION MIGRATION IN PSCs

The origin of JV hysteresis effect in perovskite solar cells is a topic still debated by scientific community. This anomalous effect is attributed to different phenomena, among the many, the pre-conditioning treatments of the device before scan, the presence of large defect density at transport layer interfaces and the ion migration aided by vacancies [8], [9].

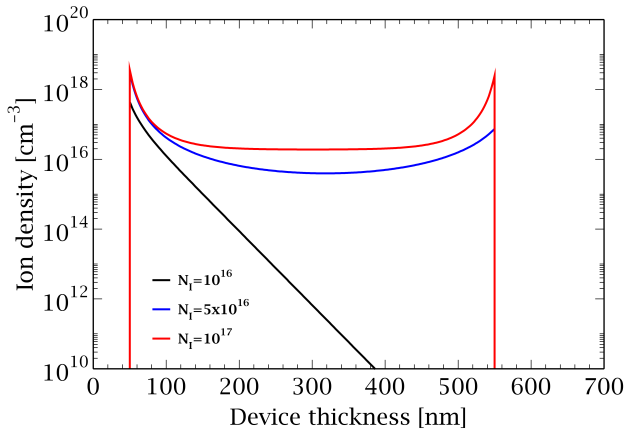
Here, we exploit the mp-DD model's ability to investigate the ion migration effect on the JV curve hysteresis. To do this, we simulated a PSC structure made by FTO/TiO₂/MAPbI₃/Spiro-OMeTAD/Au, where the 500 nm perovskite (MAPbI₃) layer works as absorber, while 50 nm-thick TiO₂ and 200 nm-thick Spiro-OMeTAD materials work respectively as electron and hole transport layer. Due to its low activation energy, the iodide ion (I^-) is the mobile specie, that we include in the mp-DD system Eq. (1) as additional transport equation. Since the response of mobile ions in MAPbI₃ is on the order of few seconds and the typical scan rates provide $V_{scan} > 0.12-0.14$ $\text{V} \cdot \text{s}^{-1}$, during both the reverse and forward scan ions have not enough time to diffuse through the perovskite layer. For this reason, we performed drift-diffusion simulations in fast-scan limit condition ($V_{scan} \gg 0.14$ $\text{V} \cdot \text{s}^{-1}$) to calculate the reverse and forward JV characteristics of the solar cell. This assumption allows us to model ions as fixed charged traps during the reverse and forward voltage sweep, and modeling them as mobile particles only at short-circuit current and at maximum applied voltage operation conditions. This is done to simulate the slow response than free carriers during the scan and their migration mechanism when the scan process stops.

Using this modeling concept, we investigated the PSC operation by varying the ion density (N_I) in the range of 1×10^{15} - 5×10^{17} cm^{-3} , and considering a diffusion coefficient of 10^{-12} $\text{cm}^2 \cdot \text{s}^{-1}$. The charge carrier generation profile is calculated from the Lambert-Beer model by assuming illumination from the cathode (FTO). We account for recombination losses, both the defect-mediated (ShockleyReadHall) and direct, by setting typical rate constant and carrier lifetimes for perovskite materials ($\tau_{SRH}=10^{-8}$ s and $C_{dir}=10^{-9}$ $\text{cm}^{-3} \cdot \text{s}^{-1}$).

Figure 3(a) shows the comparison of the most representative results obtained. While for the bottom value of N_I used there is no effect, the increase of N_I leads to have different JV curves for the reverse and forward scan. This depends on the quantity of ions accumulate at interfaces between perovskite and transport layers. Observing the substantial drop of short-circuit current density (J_{SC}) respect to the slight variation of the open-circuit voltage (V_{OC}), is clear that the ions accumulation mainly affect the device operation at J_{SC} , where the density of free carriers is lower and can be comparable with N_I . In fact, as depicted in Fig. 3(b), the more we increase N_I and greater is the ions accumulation at interfaces, thus more effective will be the hysteresis effect. Comparing the blue and red curves we can conclude that the progressive accumulation of ions at interfaces concurs to the introduction of an effective



(a)



(b)

Fig. 3. a) Reverse (full lines) and forward (dashed lines) J-V characteristics and b) ion density profile at short-circuit current density for different values of ion concentration distributed within the 500 nm thick perovskite absorber.

shunt resistance, which determines a considerable drop of the solar cell performance.

V. CONCLUSIONS

We have presented an implementation of a generalized multi-particle drift-diffusion model capable to overcome the limitations typically imposed by the two-carrier transport based drift-diffusion model. The model allows considering multiple carrier sub-populations, each assumed in thermal local equilibrium and guarantees a strictly thermodynamically consistent formulation for both the generation and recombination between populations. We proved its flexibility and ability by describing systems with different application contexts.

In Sec III we have demonstrated the model's ability on the calculation of both the charge carriers and excitons transport. The modeling of the inter-system crossing process allowed us to calculate the internal optical power emitted by a typical phosphorescent OLED structure. Then, by comparing calcula-

tions with experimental measures we have estimated the light extraction efficiency.

In Sec IV, instead, we have investigated the effect of ion migration on the perovskite solar cells performance. The inclusion of iodide ions within the MAPbI₃ absorber allowed us to calculate the transport, and concluding on their accumulation effect on the JV characteristics.

Besides the examples shown, the model presented is suitable for a wide number of systems, for which ions, excitons or electron/hole sub-populations play a fundamental role in the device behavior.

ACKNOWLEDGMENT

This work was supported by the European Unions' Horizon 2020 Research and Innovation Programme under Grant 737089 (CHIPSCOPE) and Grant 826013 (IMPRESSIVE).

REFERENCES

- [1] W van Roosbroeck. Theory of the flow of electrons and holes in germanium and other semiconductors. *Bell Labs Technical Journal*, 29(4):560–607, 1950.
- [2] Markus Kantner, Markus Mittnenzweig, and Thomas Koprucki. Hybrid quantum-classical modeling of quantum dot devices. *Physical Review B*, 96(20):205301, 2017.
- [3] Friedhard Römer and Bernd Witzigmann. Effect of auger recombination and leakage on the droop in ingan/gan quantum well leds. *Optics express*, 22(106):A1440–A1452, 2014.
- [4] Daniele Rossi, Francesco Santoni, Matthias Auf Der Maur, and Aldo Di Carlo. A multiparticle drift-diffusion model and its application to organic and inorganic electronic device simulation. *IEEE Transactions on Electron Devices*, 66(6):2715–2722, 2019.
- [5] M. Auf der Maur, G. Penazzi, G. Romano, F. Sacconi, A. Pecchia, and A. Di Carlo. The multiscale paradigm in electronic device simulation. *IEEE Transactions on Electron Devices*, 58(5):1425–1432, May 2011.
- [6] Ching W Tang and Steven A VanSlyke. Organic electroluminescent diodes. *Applied physics letters*, 51(12):913–915, 1987.
- [7] Chihaya Adachi, Marc A Baldo, Mark E Thompson, and Stephen R Forrest. Nearly 100% internal phosphorescence efficiency in an organic light-emitting device. *Journal of Applied Physics*, 90(10):5048–5051, 2001.
- [8] Henry J Snaith, Antonio Abate, James M Ball, Giles E Eperon, Tomas Leijtens, Nakita K Noel, Samuel D Stranks, Jacob Tse-Wei Wang, Konrad Wojciechowski, and Wei Zhang. Anomalous hysteresis in perovskite solar cells. *J. Phys. Chem. Lett*, 5(9):1511–1515, 2014.
- [9] Giles Richardson, Simon EJ O'Kane, Ralf G Niemann, Timo A Peltola, Jamie M Foster, Petra J Cameron, and Alison B Walker. Can slow-moving ions explain hysteresis in the current–voltage curves of perovskite solar cells? *Energy & Environmental Science*, 9(4):1476–1485, 2016.